Composites Part B 83 (2015) 153–165

Contents lists available at ScienceDirect

Composites Part B

journal homepage: www.elsevier.com/locate/compositesb

Failure analysis of fiber-reinforced composite laminates subjected to biaxial loads

Hsuan-Teh Hu [a, *], Wen-Pin Lin [b], Fang-Tai Tu [a]

[a] Department of Civil Engineering, National Cheng Kung University, Tainan 701, Taiwan, ROC
[b] Department of Civil Engineering, Chinese Military Academy, Kaohsiung 830, Taiwan, ROC

ARTICLE INFO

Article history:
Received 29 December 2014
Received in revised form
13 April 2015
Accepted 6 August 2015
Available online 21 August 2015

Keywords:
A. Laminates
C. Computational modelling
C. Finite element analysis (FEA)

ABSTRACT

A nonlinear constitutive model for a single lamina is proposed for the failure analysis of composite laminates. In the material model, both fiber and matrix are assumed to behave as elastic-plastic and the in-plane shear is assumed to behave nonlinearly with a variable shear parameter. The damage onset for individual lamina is detected by a mixed failure criterion, composed of the Tsai-Wu criterion and the maximum stress criterion. After damage takes place within the lamina, the fiber and in-plane shear are assumed to exhibit brittle behavior, and the matrix is assumed to exhibit degrading behavior. The proposed nonlinear constitutive model is tested against experimental data and good agreement is obtained. Then, numerical analyses are carried out to study the failure behavior of symmetric angle-ply composite laminates and symmetric cross-ply composite laminates subjected to biaxial loads. Finally, the conclusions obtained from the numerical analysis are given.

1. Introduction

Due to lightweight and high strength, the use of fiber-reinforced composite laminate materials (Fig. 1) in aerospace industry, mechanical industry, marine industry and offshore structures has increased rapidly in recent years. Numerous cases involving the design of composite structures show that there is a need for more refined analysis taking into account phenomena such as progressive failure and inelastic or nonlinear deformation of composite materials [1–32]. It is well known that unidirectional fibrous composites exhibit severe nonlinearity in their in-plane shear stress–strain relations [33,34]. In addition, deviation from linearity is also observed with in-plane transverse loading but the degree of nonlinearity is not comparable to that observed with the in-plane shear [35,36]. Therefore, appropriate modeling of the nonlinear behavior of fiber-reinforced composite materials becomes crucial.

A significant number of macro-mechanical models have been proposed to represent the constitutive relation of fiber-reinforced composite materials such as nonlinear elasticity models [33,35,37], plasticity models [38–42], or damage theory coupled with elasticity [43]. In addition, various failure criteria have also been proposed to predict the onset of damage in single layer within fiber-reinforced composites, i.e. limit theories [44], polynomial theories [45,46], and direct mode-determining theories [3,47–49]. As for the post-damage process of individual lamina, two idealized types of failure modes have been defined in a previous study [41]; namely, brittle and ductile. In the case of the brittle mode, the material is assumed to give up its entire stiffness and strength in the dominant stress direction as the damage is reached, whereas for the ductile mode, the material retains its strength but loses its overall stiffness in the direction of damage.

Obviously, a rational analysis of the individual layer within the laminate under loading must include three parts; i.e., pre-damage analysis, damage onset determination, and post-damage analysis. In the pre-damage analysis, the material response of the lamina is modeled by an elastic-plastic behavior in both the fiber direction and transverse direction of the lamina. However, the in-plane shear is assumed to behave nonlinearly with a variable shear parameter. For the damage onset determination of individual lamina, the Tsai-Wu failure criterion [27,46,50] is the most common criterion used in the past. However, Lin and Hu [11,12] point out that the Tsai-Wu failure criterion would cause overestimated failure stresses in the fiber direction of the composite lamina. To eliminate this unreasonable phenomenon, an extra limitation should be added into the Tsai-Wu failure criterion to obtain a more accurate and reasonable stresses in the composite lamina. As the results, Lin and Hu [11,12]

* Corresponding author. Tel.: +886 6 2757575x63168; fax: +886 6 2358542.
E-mail address: hthu@mail.ncku.edu.tw (H.-T. Hu).

http://dx.doi.org/10.1016/j.compositesb.2015.08.045
1359-8368/

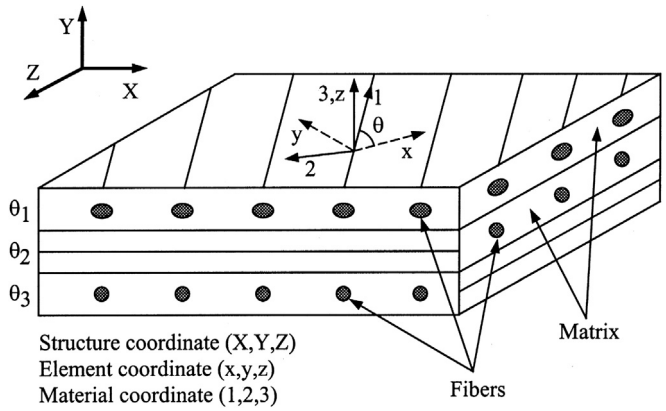

Fig. 1. Material, element and structure coordinates of fiber reinforced plastics.

and Zhu and Sankar [51] suggested that the combination of both the Tsai-Wu criterion and the maximum stress criterion, which is called the mixed criterion, was a much better criterion for determining the damage to lamina. Thus, in this paper, a mixed criterion is employed to determine the damage onset of individual layer within the laminate under loading. For the post-damage analysis, a degrading mode for matrix and brittle modes for fiber and in-plane shear are used to simulate the post damage behavior of individual lamina.

In this paper, the nonlinear constitutive model of fiber-reinforced composite laminate materials, involving pre-damage analysis, damage onset determination, and post-damage analysis, is reviewed. Then, the Abaqus finite element program [52] is used to verify the proposed constitutive model against experimental data. In addition, numerical analyses of composite laminates with symmetric angle-ply and symmetric cross-ply subjected to biaxial loads are carried out. Finally, the conclusions obtained from the numerical analysis are given.

2. Nonlinear analysis model

2.1. Stress–strain curves and post damage models

For a single lamina subjected to tensile loading, the stress–strain curves of the nonlinear analysis model are shown in Fig. 2a and c. It is assumed that the material response can be represented by elastic-plastic stress–strain curves in the principal material directions, i.e. the 1 direction (fiber direction) and the 2 direction (transverse direction), of the lamina. Let X_{yt} and X_{ut} be the yield strength and the ultimate strength of the lamina for tension in the 1 direction, Y_{yt} and Y_{ut} be the yield strength and the ultimate strength of the lamina for tension in the 2 direction. For the elastic regions, i.e. $\sigma_1 \le X_{yt}$ and $\sigma_2 \le Y_{yt}$, the elastic moduli are denoted by E_{iie} ($i = 1,2$). For the plastic regions, i.e. $X_{yt} \le \sigma_1 \le X_{ut}$ and $Y_{yt} \le \sigma_2 \le Y_{ut}$, the elastic moduli are denoted by E_{iipt} ($i = 1,2$). For a lamina subjected to compressive

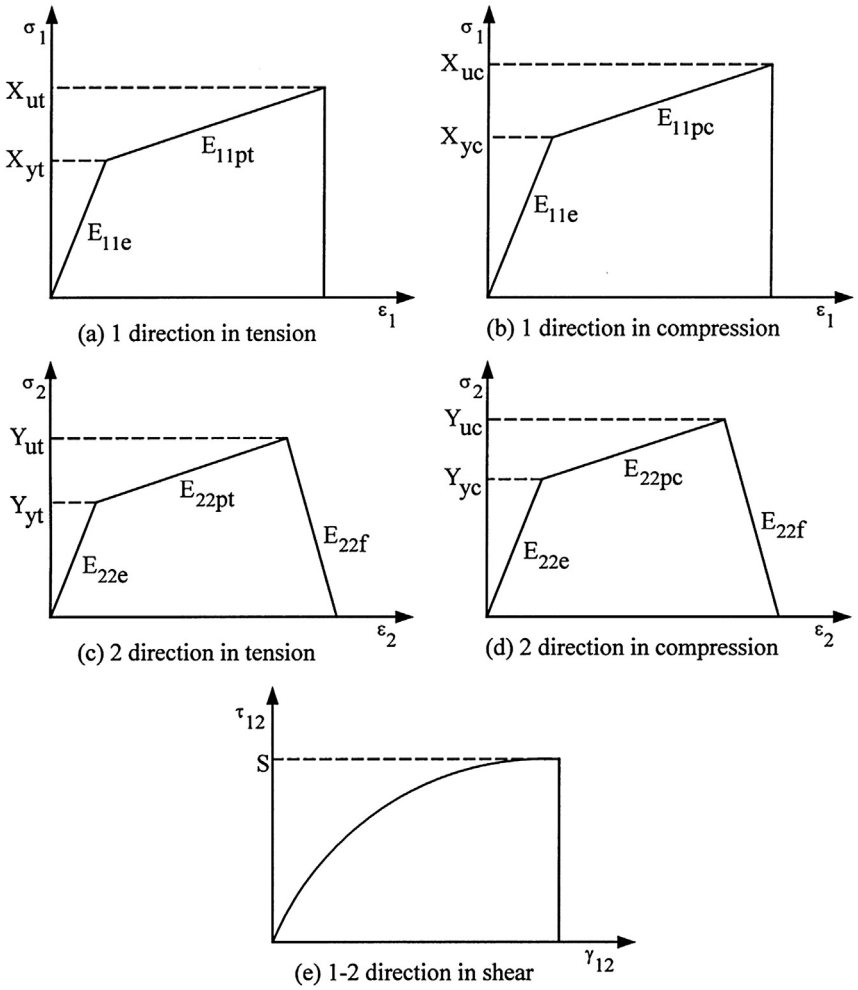

Fig. 2. Stress–strain curves of the proposed nonlinear failure model.

loading, the stress–strain curves are shown in Fig. 2b and d. It is obvious that X_{yc} and X_{uc} are the yield strength and the ultimate strength of the lamina for compression in the 1 direction and that Y_{yc} and Y_{uc} are the yield strength and the ultimate strength of the lamina for compression in the 2 direction. For the plastic regions, i.e. $X_{yc} \le \sigma_1 \le X_{uc}$ and $Y_{yc} \le \sigma_2 \le Y_{uc}$, the elastic moduli are denoted by E_{iipc} (i = 1,2). Let S be the ultimate in-plane shear strength. It is assumed that the in-plane shear in the 1–2 direction can be modeled by a nonlinear stress–strain curve as shown in Fig. 2e.

In the post-damage region, the strengths drop to zero (brittle modes) for normal stress in the 1 direction (Fig. 2a and b) and the shear stress in the 1–2 direction (Fig. 2e). However, the elastic stiffness is assumed to have a negative modulus E_{22f} (degrading mode) for normal stress in the 2 direction (Fig. 2c and d). This means that the damaged lamina unloads in the transverse direction through a negative tangent modulus until no load remains in the lamina.

2.2. Nonlinear constitutive model of the lamina

For fiber-composite laminate materials, each lamina can be considered to be an orthotropic layer in a plane stress condition. Taking into account the elastic-plastic behavior in the 1 and 2 directions and the nonlinear behavior on the 1–2 plane within the lamina, the strain–stress relations for an orthotropic lamina in the material coordinates (1,2) can be written as [33]:

$$\begin{Bmatrix} \varepsilon_1 \\ \varepsilon_2 \\ \gamma_{12} \end{Bmatrix} = \begin{bmatrix} \frac{1}{E_{11}} & \frac{-\nu_{21}}{E_{22}} & 0 \\ \frac{-\nu_{12}}{E_{11}} & \frac{1}{E_{22}} & 0 \\ 0 & 0 & \frac{1}{G_{12}} \end{bmatrix} \begin{Bmatrix} \sigma_1 \\ \sigma_2 \\ \tau_{12} \end{Bmatrix} + S_{6666}\tau_{12}^2 \begin{Bmatrix} 0 \\ 0 \\ \tau_{12} \end{Bmatrix} \tag{1}$$

where ε_1, ε_2, and γ_{12} represent the strains in the 1 direction, 2 direction and the 1–2 plane, respectively. σ_1, σ_2 and τ_{12} denote the stresses in the 1-direction, 2-direction and the 1–2 plane, respectively. The ν_{12} and ν_{21} are the Poisson's ratios, and E_{11} and E_{22} are the elastic moduli in the 1 and 2 directions. If the lamina is in the elastic stage in the 1 or 2 direction, then $E_{11} = E_{11e}$ or $E_{22} = E_{22e}$. If the lamina is in the plastic stage in the 1 or 2 direction, then $E_{11} = E_{11pt}$ or $E_{11} = E_{11pc}$ and $E_{22} = E_{22pt}$ or $E_{22} = E_{22pc}$. The G_{12} is the shear modulus, and S_{6666} is a shear parameter to account for the in-plane shear nonlinearity. The value of S_{6666} can be determined by a curve fit to pure shear test data.

The incremental stress–strain relations for a nonlinear orthotropic lamina can be given as follows:

$$\Delta\{\sigma'\} = [Q_1']\Delta\{\varepsilon'\} \tag{2}$$

$$\Delta\{\tau_t'\} = [Q_2']\Delta\{\gamma_t'\} \tag{3}$$

where $\Delta\{\sigma'\} = \Delta\{\sigma_1,\sigma_2,\tau_{12}\}^T$; $\Delta\{\tau_t'\} = \Delta\{\tau_{13},\tau_{23}\}^T$; $\Delta\{\varepsilon'\} = \Delta\{\varepsilon_1,\varepsilon_2,\gamma_{12}\}^T$; $\Delta\{\gamma_t'\} = \Delta\{\gamma_{13},\gamma_{23}\}^T$ and

$$[Q_1'] = \begin{bmatrix} \frac{E_{11}}{1-\nu_{12}\nu_{21}} & \frac{\nu_{12}E_{22}}{1-\nu_{12}\nu_{21}} & 0 \\ \frac{\nu_{21}E_{11}}{1-\nu_{12}\nu_{21}} & \frac{E_{22}}{1-\nu_{12}\nu_{21}} & 0 \\ 0 & 0 & \frac{1}{1/G_{12}+3S_{6666}\tau_{12}^2} \end{bmatrix} \tag{4}$$

$$[Q_2'] = \begin{bmatrix} \alpha_1 G_{13} & 0 \\ 0 & \alpha_2 G_{23} \end{bmatrix} \tag{5}$$

The terms α_1 and α_2 are the shear correction factors [53] and they are taken to be 0.83 in this study. It is assumed that the transverse shear stresses always behave linearly and do not affect the nonlinear in-plane behavior of individual lamina.

2.3. Failure criterion and degradation of stiffness

The maximum stress criterion is the dominant member of the limit failure theory category [44]. For the plane stress condition, the maximum stress criterion for an orthotropic material can be expressed as follows:

$$\frac{\sigma_1}{X_{ut}} = 1 \quad \text{or} \quad \frac{\sigma_1}{X_{uc}} = 1 \tag{6}$$

$$\frac{\sigma_2}{Y_{ut}} = 1 \quad \text{or} \quad \frac{\sigma_2}{Y_{uc}} = 1 \tag{7}$$

$$\frac{\tau_{12}}{S} = 1 \tag{8}$$

The Tsai-Wu failure criterion has a general nature, because it contains almost all other polynomial theories as special cases. Under the plane stress condition, the Tsai-Wu failure criterion has the following form [46]:

$$F_1\sigma_1+F_2\sigma_2+F_{11}\sigma_1^2+2F_{12}\sigma_1\sigma_2+F_{22}\sigma_2^2+F_{66}\tau_{12}^2 = 1 \tag{9a}$$

where

$$F_1 = \frac{1}{X_{ut}}+\frac{1}{X_{uc}}, \quad F_{11} = \frac{1}{X_{ut}X_{uc}}, \quad F_2 = \frac{1}{Y_{ut}}+\frac{1}{Y_{uc}}$$
$$F_{22} = \frac{1}{Y_{ut}Y_{uc}}, \quad F_{66} = \frac{1}{S^2} \tag{9b}$$

The stress interaction term F_{12} in Eq. (9a) is difficult to determine and Narayanaswami and Adelman [54] suggested that F_{12} could be set equal to zero for practical engineering applications. Therefore, $F_{12} = 0$ is used in this study.

Although the Tsai-Wu failure criterion is widely used in determining the damage onset of a lamina, there are some drawbacks with it. Among them is the fact that the failure stress of a fiber in a lamina may exceed the strength of the material in the case of symmetric angle-ply laminates with a small fiber angle (say $0^\circ < \theta < 20^\circ$) subjected to off-axis tension [11]. In order to eliminate this unreasonable phenomenon, the limitation of the maximum stress of the lamina in the fiber direction is added into the Tsai-Wu failure criterion to obtain a mixed failure criterion [11,12,51], which has the following formulations:

$$F_1\sigma_1+F_2\sigma_2+F_{11}\sigma_1^2+F_{22}\sigma_2^2+F_{66}\tau_{12}^2 = 1 \tag{10a}$$

and

$$\frac{\sigma_1}{X_{ut}} \le 1 \quad \text{or} \quad \frac{\sigma_1}{X_{uc}} \le 1 \tag{10b}$$

2.4. Degradation models

Upon damage within the lamina occurring, the material properties begin to degrade. According to the literature, the degradation

models for each layer can be separated into three types, i.e. the brittle, ductile [41] and degrading modes [11,12]. For the brittle mode, the material is assumed to lose its entire stiffness and strength in the dominant stress direction. For the ductile mode the material retains its strength but loses all of its stiffness in the failure direction. For the degrading mode the material is assumed to lose its stiffness and strength in the failure direction gradually until the stress in that direction is reduced to zero.

In this investigation, it is assumed that the post damage modes are idealized as the brittle behavior for σ_1 and τ_{12} and the degrading behavior for σ_2 (Fig. 2). The following three rules are used to determine whether the ply failure is caused by matrix fracture, shear failure, or fiber fracture [2]:

(1) If a ply fails in the condition of $X_{uc} < \sigma_1 < X_{ut}$, and $-S < \tau_{12} < S$, the damage is assumed to be matrix induced. Consequently, the degradation of transverse stiffness occurs. Due to the interlock action with the neighboring plies, the damaged ply gradually loses its capability to support transverse stress. The lamina remains able to carry the longitudinal and shear stresses. In this case, the constitutive matrix of the lamina can be written as

$$[Q_1'] = \begin{bmatrix} E_{11} & 0 & 0 \\ 0 & E_{22f} & 0 \\ 0 & 0 & \dfrac{1}{1/G_{12} + 3S_{6666}\tau_{12}^2} \end{bmatrix} \tag{11}$$

where E_{22f} is a negative tangent modulus in the transverse direction of the lamina after matrix damage. In the proposed model, the shear parameter S_{6666} has a variable value.

(2) If the ply fails in the condition of $X_{uc} < \sigma_1 < X_{ut}$, and $\tau_{12} \geq S$ or $\tau_{12} \leq -S$, the damage is assumed to be shear induced. Consequently, the damaged lamina loses its capability to support transverse and shear stresses, but remains able to carry longitudinal stress. In this case, the constitutive matrix of the lamina becomes

$$\left[Q_1'\right] = \begin{bmatrix} E_{11} & 0 & 0 \\ 0 & 0 & 0 \\ 0 & 0 & 0 \end{bmatrix} \tag{12}$$

(3) If the ply fails with $\sigma_1 \geq X_{ut}$, or $\sigma_1 \leq X_{uc}$, the ply failure is caused by fiber fracture and a total ply rupture is assumed. Thus, the constitutive matrix of the lamina becomes

$$[Q_1'] = \begin{bmatrix} 0 & 0 & 0 \\ 0 & 0 & 0 \\ 0 & 0 & 0 \end{bmatrix} \tag{13}$$

3. Laminate governing equations

The forgoing nonlinear failure analysis model for fiber-reinforced composite lamina can be combined with classical lamination theory to form the following incremental laminate force–strain relations:

$$\Delta\{N\} = \sum_{i=1}^{n} [Q]_i t_i \Delta\{\varepsilon\} \tag{14}$$

where $\Delta\{N\} = \Delta\{N_x, N_y, N_{xy}\}^T$ and $\Delta\{\varepsilon\} = \Delta\{\varepsilon_x, \varepsilon_y, \gamma_{xy}\}^T$ are the vectors of the incremental in-plane forces and the incremental strains in the overall laminate coordinate system (x,y), respectively. The term t_i is the thickness of the i-th layer; n is the total number of layers. The matrix $[Q]_i$ stands for constitutive matrix for the i-th layer and can be obtained by proper rotation of the $[Q_1']$ matrix of that layer [2].

4. Numerical analysis

4.1. Verification of the proposed constitutive model

The validity of the proposed constitutive model for composite laminates subjected to uniaxial tensile load and uniaxial compressive load has been verified by Lin and Hu [11] and Ke [55]. In this session, the proposed constitutive model is tested against experimental data [56] of composite laminates subjected to biaxial loads. The composite laminates are composed of E-glass fiber (Silenka 051L, 1200 tex) and an epoxy resin system (Ciba–Geigy MY 750/HY 917/DY 063). It is known that polymer composites do not have a bi-linear (hardening) behavior when loaded in the longitudinal direction, nor under transverse tension. The proposed constitutive model can be easily implemented to polymer composites by setting $E_{11e} = E_{11pt} = E_{11pc}$, $E_{22e} = E_{22pt} = E_{22pc}$, $X_{yt} = X_{ut}$, $X_{yc} = X_{uc}$, $Y_{yt} = Y_{ut}$, $Y_{yc} = Y_{uc}$.

For the purpose of verification, the material constants provided by Soden, Hinton and Kaddour [57] are used in the analyses. They are listed as follow: $E_{11e} = E_{11pt} = E_{11pc} = 45.6$ GPa, $E_{22e} = E_{22pt} = E_{22pc} = 16.2$ GPa, $E_{22f} = -4.02$ GPa, $G_{12} = 5.83$ GPa, $\nu_{12} = 0.278$, $X_{yt} = X_{ut} = 1280$ MPa, $X_{yc} = X_{uc} = -800$ MPa, $Y_{yt} = Y_{ut} = 40$ MPa, $Y_{yc} = Y_{uc} = -145$ MPa, $S = 72$ MPa. The shear parameter S_{6666} is obtained by curve fitting from the pure shear test data of Soden, Hinton and Kaddour [57] and is shown in Fig. 3. Its expressions are:

$$S_{6666} = \begin{cases} 0 \text{ GPa}^{-3}, & 0 \leq \gamma_{12} \leq 0.006 \\ 9724(\gamma_{12} - 0.006) \text{ GPa}^{-3}, & 0.006 \leq \gamma_{12} \leq 0.007 \\ -3.569 + 1899\gamma_{12} \text{ GPa}^{-3}, & 0.007 \leq \gamma_{12} \leq 0.04 \end{cases} \tag{15}$$

The aforementioned nonlinear constitutive model combined with mixed failure criteria and post damage modes for composite materials is written into a FORTRAN subroutine and linked to the Abaqus finite element program [52]. Since the stress field is uniform throughout the composite laminate, size effect is not crucial. The composite laminate in the analysis is shown in Fig. 4 and is assumed to be simply supported around all edges. The length of the plate L is equal to 10 cm and the width of the plate W is also equal to 10 cm. The composite laminate contains 4 plies with the thickness t of each ply equal to 0.1 mm. Only one eight-node isoparametric shell elements with six degrees of freedom per node (three displacements and three rotations) is used to model the entire composite laminate. The reduced integration rule together with hourglass stiffness control is employed to formulate the element stiffness matrix [52].

In the Abaqus program, the load control scheme with the Newton method is used in tracing the load–displacement curves of the laminates [52]. Stresses and strains in material coordinates (1,2,3) are calculated at each incremental step, and are evaluated by the failure criteria to determine both the occurrence of failure and the mode of failure. Mechanical properties of each lamina in the damaged area are reduced, according to proper degradation models. Stresses and strains are then recalculated to determine any additional damage as a result of stress redistribution at the same

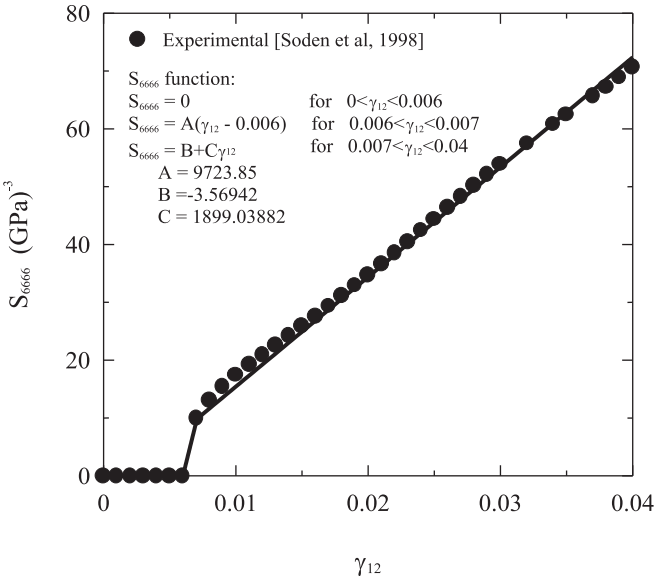

Fig. 3. Curve fitting of shear parameter S_{6666} from the pure shear test data of Soden, Hinton and Kaddour [36].

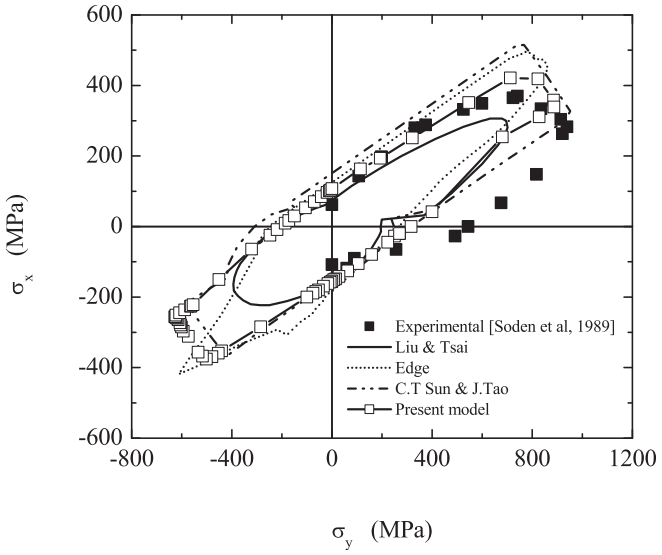

Fig. 5. Failure envelopes of biaxial stresses for $[\pm 55]_s$ composite laminate.

load. This procedure continues until no additional damage is found. Then, the next increment of load is pursued. The final collapse load is determined when the composite plates can not sustain any additional load.

Fig. 5 shows the failure envelopes of biaxial stresses for $[\pm 55]_s$ composite laminate predicted by the proposed material model, Edge model [3], Liu and Tsai model [5], and Sun and Tao model [6] against the experimental data [56]. For the biaxial tension zone, it can be seen that the failure envelope predicted by the proposed model is closer to the experimental data than the remaining models. For the biaxial tension-compression zones except the Liu and Tsai model, the failure envelopes predicted by the remaining models are close together and have reasonably good agreement with the test data. For the biaxial compression zone, there are no experimental data available. However, we know that the failure envelope in the biaxial compression zone should be similar and smaller to that in the biaxial tension zone. This is due to $X_{uc}(-800\ \text{MPa})$ of the lamina is smaller than $X_{ut}(1280\ \text{MPa})$ of the same lamina in magnitude. In the biaxial compression zone, we can see that the failure envelopes predicted by the proposed model and the Sun and Tao model are very close to each other.

It is known that there are many factors that influence the experimental results and that can not be all simulated in the numerical model. From the aforementioned discussion, it can be concluded that the proposed material model can predict the biaxial failure stresses of composite laminates with reasonably good accuracy.

4.2. Composite laminates with symmetric angle-ply subjected to biaxial compression

In this section, composite laminates with symmetric angle-ply $[\pm\theta]_s$ subjected to biaxial compressions are investigated, where $\theta = 0°, 15°, 30°, 45°$. Let the variable SR represent the stress ratio between σ_x and σ_y, i.e. $SR = \sigma_x/\sigma_y$. Typical loading paths of composite laminates for various SR ratios are shown in Fig. 6. Fig. 7 shows the stress and strain relations for $[\pm 0]_s$ composite laminates subjected to biaxial compressions. From Fig. 7, it can be seen

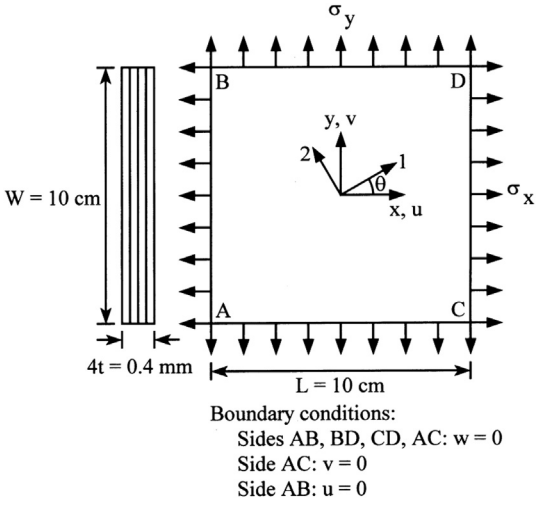

Fig. 4. Geometry and boundary conditions of composite laminates.

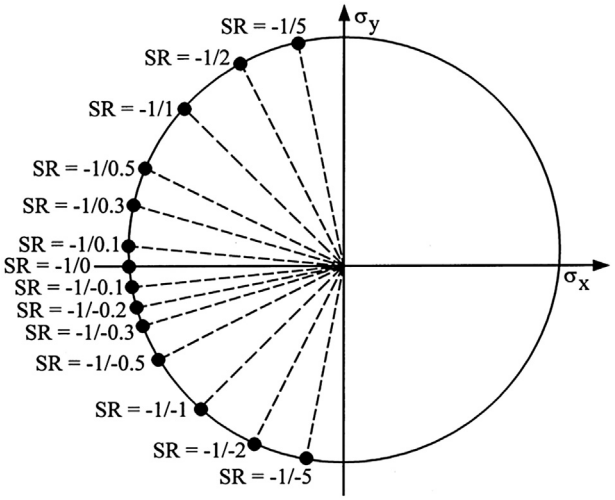

Fig. 6. Typical loading paths of composite laminates for various SR ratios.

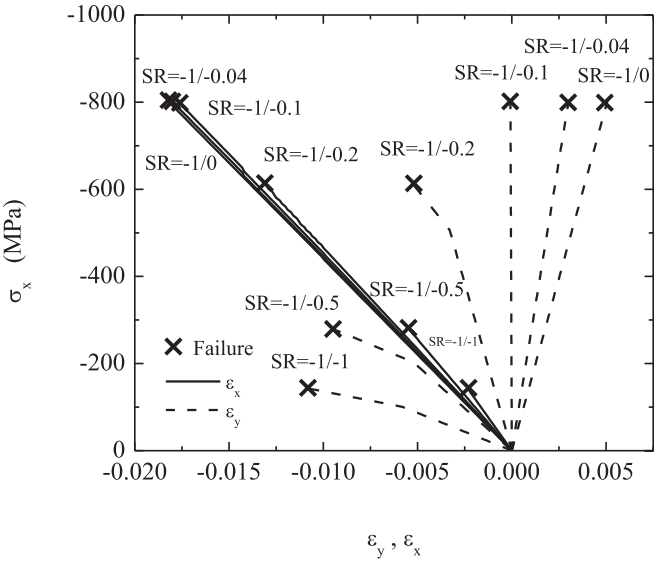

Fig. 7. Stress–strain curves of $[\pm 0]_s$ composite laminates subjected to biaxial compressions.

that when SR = −1/0, −1/−0.04 and −1/−0.1, the stress–strain curves of the $[\pm 0]_s$ laminates are quite linear. The failure modes of these laminates are all fiber compressive failures and the ultimate strengths of these laminates are very close to X_{uc}(−800 MPa). When SR = −1/−0.2, −1/−0.5 and −1/−1, the stress–strain curves of the laminates are also quite linear in the x direction but exhibit nonlinear behavior in the y direction. The failure modes of these laminates change from fiber compressive failure (SR = −1/−0.2), combined fiber and matrix failure (SR = −1/−0.5) to matrix failure in compression (SR = −1/−1). The ultimate strengths of these laminates are reduced with the increase of the magnitude of the compressive stress σ_y.

Fig. 8 shows the stress and strain relations for $[\pm 15]_s$ composite laminates subjected to biaxial compressions. When SR = −1/0, the failure mode of the laminate is a combined fiber, matrix and shear failure. When SR = −1/−0.04 and −1/−0.1, the failure modes of these laminates are combined fiber and shear failures. This is due to the increase of the in-plane shear in those laminates. In these stress ratio regions, the stress–strain curves of the laminates are quite linear and the ultimate strengths of the laminates increase with the increase of the magnitude of compressive stress σ_y. When SR = −1/−0.2, −1/−0.5 and −1/−1, the transverse stress in the matrix becomes more significant in the laminate. Hence, the failure modes of these laminates become matrix failures in compression. As a result, the ultimate strengths of these laminates reduce with the increase of the magnitude of compressive stress σ_y. The stress–strain curves of these laminate are also quite linear in the x direction but exhibit nonlinear behavior in the y direction.

Fig. 9 shows the stress and strain relations for $[\pm 30]_s$ composite laminates subjected to biaxial compressions. When SR = −1/0, −1/−0.04 and −1/−0.1, the matrixes of the laminates fail in compression first which is called initial failure. Although, the transverse stresses in the matrixes are gradually reduced (Fig. 2d), these laminates can still resist the biaxial loads until the in-plane shear failure occurs, which is termed a final failure. When SR = −1/−0.3, there is no initial failure. The (final) failure mode of the laminate is a combined fiber and shear failure. When SR = −1/−0.33 and −1/−0.5, the initial failures of the laminates occur due to matrix failure in compression. The final failures of the laminates occur when the fibers also fail in compression. When SR = −1/−1, the initial failure of the laminate occurs due to matrix failure in compression. The final failure of the laminate occurs when the transverse stress in the matrix is reduced to zero (Fig. 2d). From this figure, we can observe that when SR is between −1/0 and −1/−0.33, the ultimate strengths of the laminates increase with the increase of the magnitude of compressive stress σ_y. However, when SR is between −1/−0.33 and −1/−1, the ultimate strengths of the laminates decrease with the increase of the magnitude of compressive stress σ_y. The stress–strain curves of these laminates exhibit highly nonlinear behavior in the y direction due to the nonlinear shear effect.

Fig. 10 shows the stress and strain relations for $[\pm 45]_s$ composite laminates subjected to biaxial compressions. When SR = −1/0 and −1/−0.1, there is no initial failure. The (final) failure mode of the laminate is due to shear failure. When SR = −1/−0.5, the initial failure of the laminate occurs due to matrix failure in compression. The final failure of the laminate occurs when the shear failure takes place. When SR = −1/−1, the initial failure of the laminate occurs

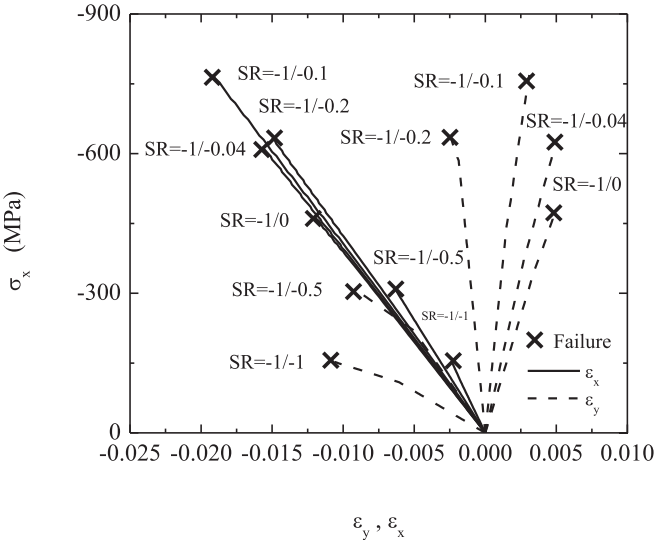

Fig. 8. Stress–strain curves of $[\pm 15]_s$ composite laminates subjected to biaxial compressions.

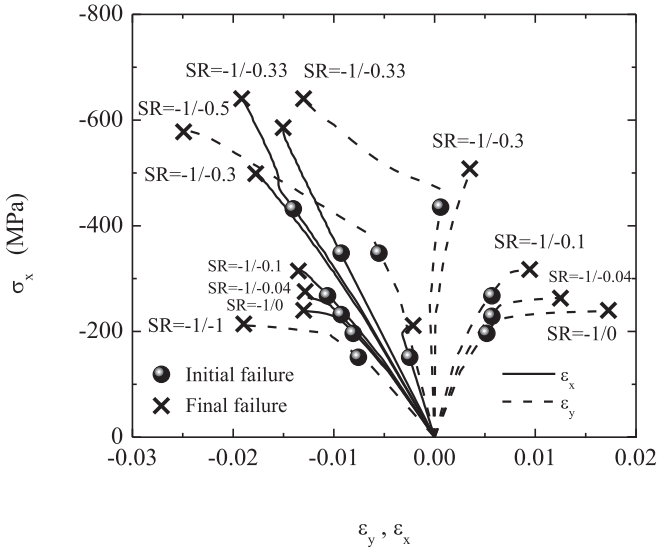

Fig. 9. Stress–strain curves of $[\pm 30]_s$ composite laminates subjected to biaxial compressions.

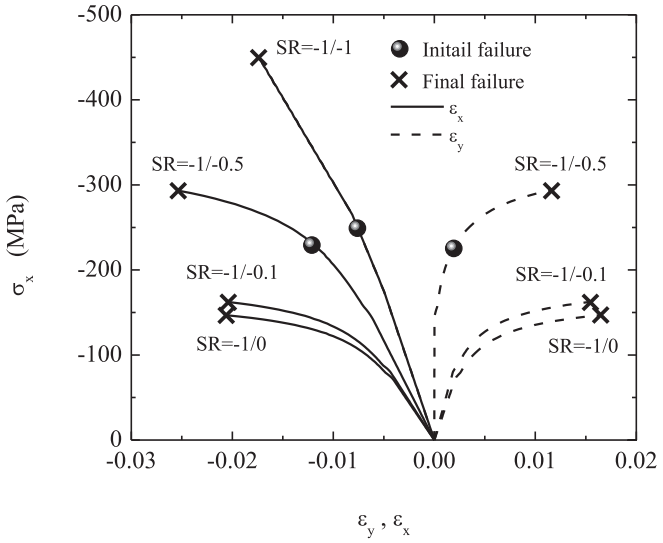

Fig. 10. Stress–strain curves of $[\pm 45]_s$ composite laminates subjected to biaxial compressions.

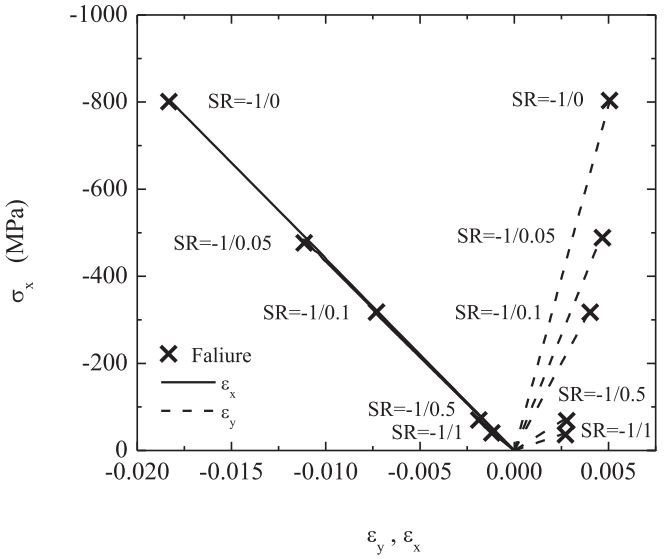

Fig. 12. Stress–strain curves of $[\pm 0]_s$ composite laminates subjected to biaxial tension and compression.

due to matrix failure in compression. The final failure of the laminate occurs when the fiber fails in compression too. From this figure, we can observe that the ultimate strengths of the laminates increase with the increase of the magnitude of compressive stress σ_y. The stress–strain curves of these laminates exhibit highly nonlinear behavior both in the x and y directions. The reason is that the nonlinear in-plane shear effect is the most significant in $[\pm 45]_s$ laminates than in other laminates.

Fig. 11 shows the failure stress σ_{xf} in the x direction versus the fiber angle θ for composite laminates with $[\pm\theta]_s$ layup. It can be seen that the optimal fiber angle of the laminate change from 0° to 90°, as the SR ratio changes from −1/0 to −1/−25. Generally, the optimal fiber angle increases with the increase of the magnitude of compressive stress σ_y. For example, when SR = −1/0, the optimal angle is 0°. When SR = −1/−1, the optimal angle is 45°. When SR = −1/−25, the optimal angle is 90°. When θ = 0° or 75° ≤ θ ≤ 90°, the failure stress decreases with the increase of the magnitude of compressive stress σ_y. When 5° ≤ θ ≤ 70°, the failure stress depends on the SR ratio significantly.

4.3. Composite laminates with symmetric angle-ply subjected to biaxial tension and compression

In this section, composite laminates with symmetric angle-ply $[\pm\theta]_s$ subjected to biaxial tension and compression are investigated. Typical loading paths of composite laminates for various SR ratios are shown in Fig. 6. Fig. 12 shows the stress and strain relations for $[\pm 0]_s$ composite laminates. It can be seen that all the stress–strain curves of the laminates with different SR ratios exhibit linear behavior both in the x and y directions. In addition, there are no initial failures for all the laminates. When SR = −1/0, the (final) failure of the laminate is caused by fiber failure in compression. When SR = −1/0.05, the failure mode of the laminate is a combined fiber and matrix failure. As the SR ratio is gradually

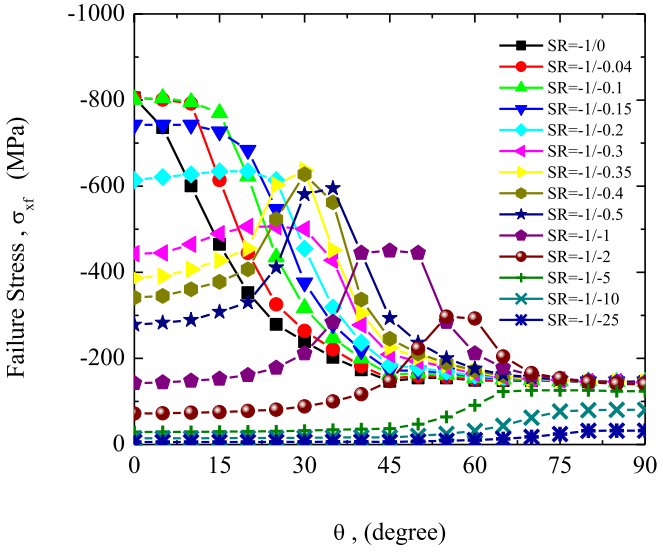

Fig. 11. Failure stress σ_{xf} versus angle θ for $[\pm\theta]_s$ composite laminates subjected to biaxial compressions with various SR ratios.

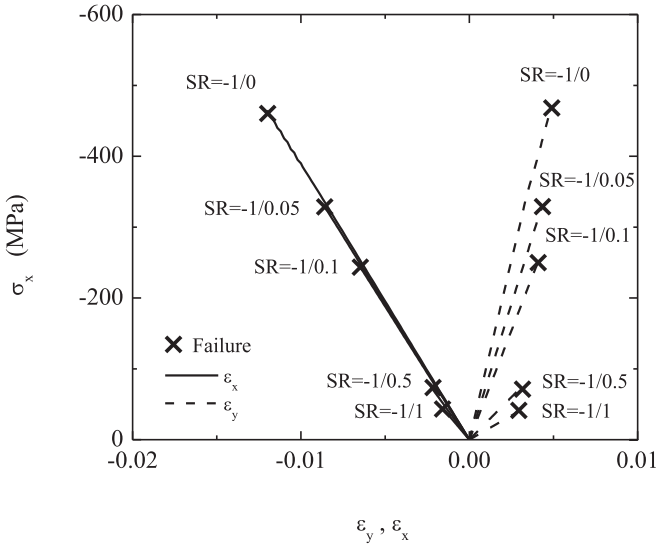

Fig. 13. Stress–strain curves of $[\pm 15]_s$ composite laminates subjected to biaxial tension and compression.

changed toward SR = −1/1, the failure modes of the laminates also change toward the matrix failure in tension. This is because the ultimate tensile strength of the matrix Y_{ut}(40 MPa) is much lower than the ultimate compressive strength of the fiber X_{uc}(−800 MPa) in magnitude. Finally, we can observe that the ultimate strengths of the laminates decrease with the increase of the magnitude of tensile stress σ_y.

Fig. 13 shows the stress and strain relations for $[\pm 15]_s$ composite laminates subjected to biaxial tension and compression. We can see that Fig. 13 is similar to Fig. 12. All the stress–strain curves of the laminates with different SR ratios exhibit linear behavior both in the x and y directions. The ultimate strengths of the laminates decrease with the increase of the magnitude of tensile stress σ_y. In addition, there are no initial failures for all the laminates. The only differences are the failure modes. Due to the fiber angles ±15°, in-plane shear stresses develop in these laminates. Hence, when SR = −1/0.05 and −1/0.1, the failures of the laminates change to the combined fiber, matrix and shear failure.

Fig. 14 shows the stress and strain relations for $[\pm 30]_s$ composite laminates subjected to biaxial tension and compression. Again, the ultimate strengths of the laminates decrease with the increase of the magnitude of tensile stress σ_y. For all the laminates, initial failures take place when the matrixes fail in tensions. These laminates can still resist further loadings but start to exhibit highly nonlinear behaviors due to the nonlinear in-plane shear effect. Final failures of all the laminates occur when the in-plane shear stresses exceed the ultimate strength S (72 MPa).

Fig. 15 shows the stress and strain relations for $[\pm 45]_s$ composite laminates subjected to biaxial tension and compression. Since the failures of these laminates are governed by the in-plane shear stress, there are no initial failures for all the laminates. Hence, final failures of these laminates are caused by the in-plane shear failures. Due to the nonlinear in-plane shear effect, these laminates exhibit highly nonlinear behaviors. Again, the ultimate strengths of the laminates decrease with the increase of the magnitude of tensile stress σ_y.

Fig. 16 shows the failure stress σ_{xf} in the x direction versus the fiber angle θ for composites with a $[\pm\theta]_s$ layup. It can be seen that the optimal fiber changes from 0° to 90°, as the SR ratio changes from −1/0 to −1/20. In addition, the failure stress decreases with the increase of the magnitude of tensile stress σ_y. This decrease of the failure stress in magnitude is more significant for small angles (say $0° \le \theta \le 15°$) than that for large angles (say $75° \le \theta \le 90°$).

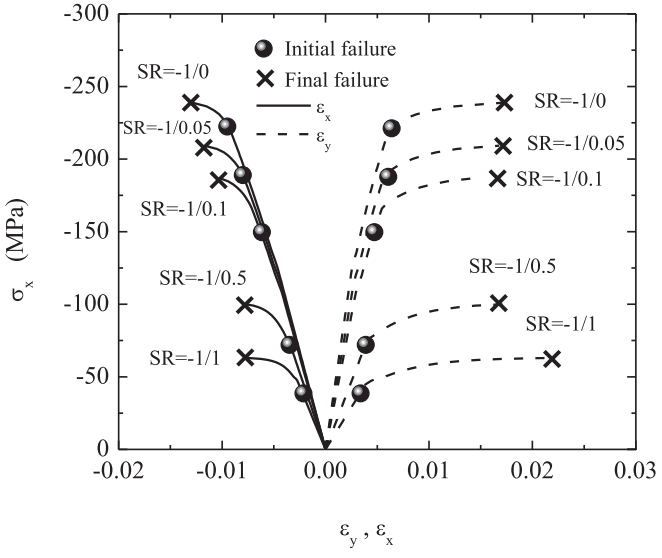

Fig. 14. Stress–strain curves of $[\pm 30]_s$ composite laminates subjected to biaxial tension and compression.

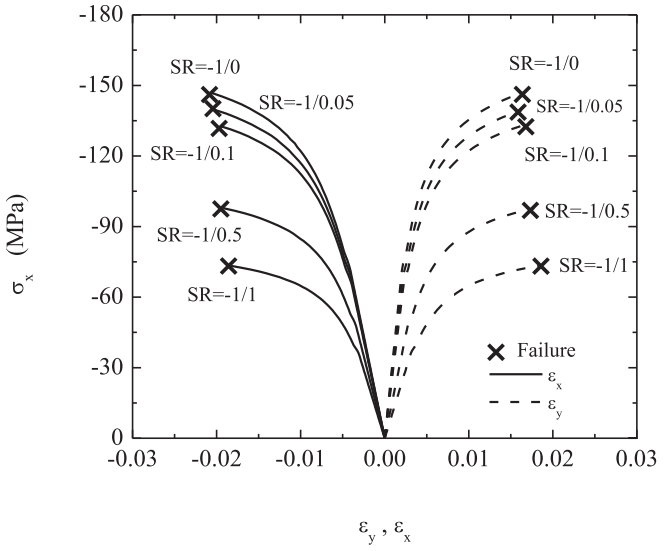

Fig. 15. Stress–strain curves of $[\pm 45]_s$ composite laminates subjected to biaxial tension and compression.

4.4. Failure envelopes of biaxial stresses for composite laminates with symmetric angle-ply

The stress–strain curves and failure patterns of the composite laminates with symmetric angle-ply $[\pm\theta]_s$ subjected to biaxial tensions are similar to those of the laminates subjected to biaxial compressions as discussed in Section 4.2. Hence, they are not duplicated here. However, it should be noted that the ultimate strengths of the laminates subjected to biaxial tensions are larger than those of the same laminates subjected to biaxial compressions due to X_{ut}(1280 MPa) of the lamina being larger than X_{uc}(−800 MPa) of the same lamina in magnitude.

Finally, the failure envelopes of biaxial stresses for composite laminates with symmetric angle-ply $[\pm\theta]_s$ are given in Fig. 17. It can

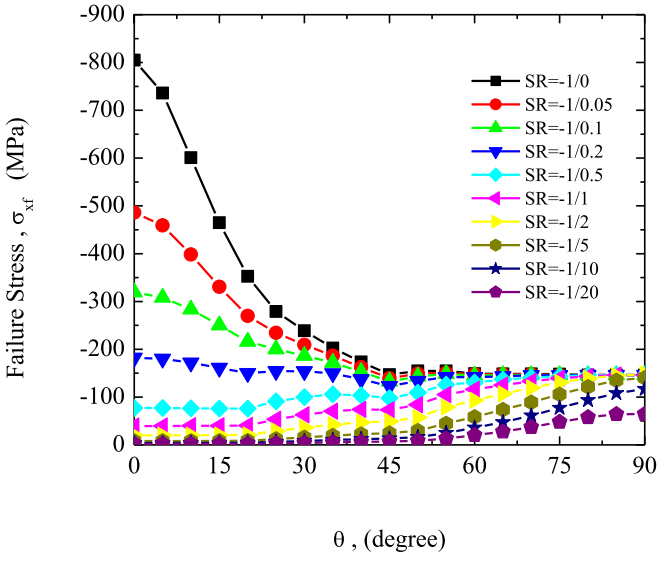

Fig. 16. Failure stress σ_{xf} versus angle θ for $[\pm\theta]_s$ composite laminates subjected to biaxial tension and compression with various SR ratios.

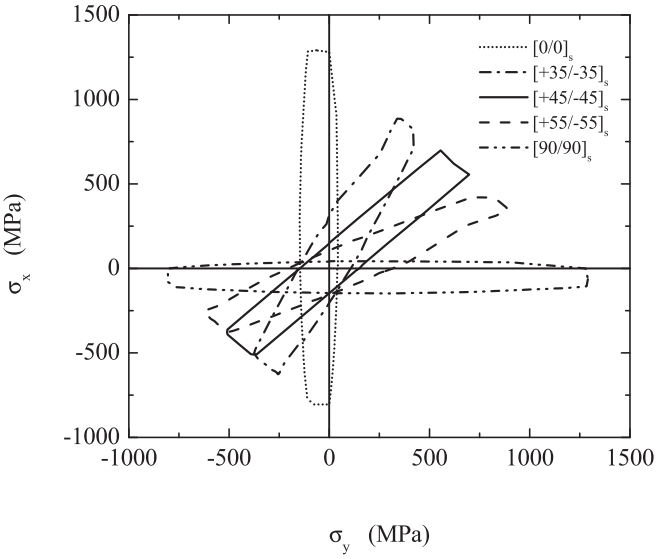

Fig. 17. Failure envelopes of biaxial stresses for $[\pm\theta]_s$ composite laminates.

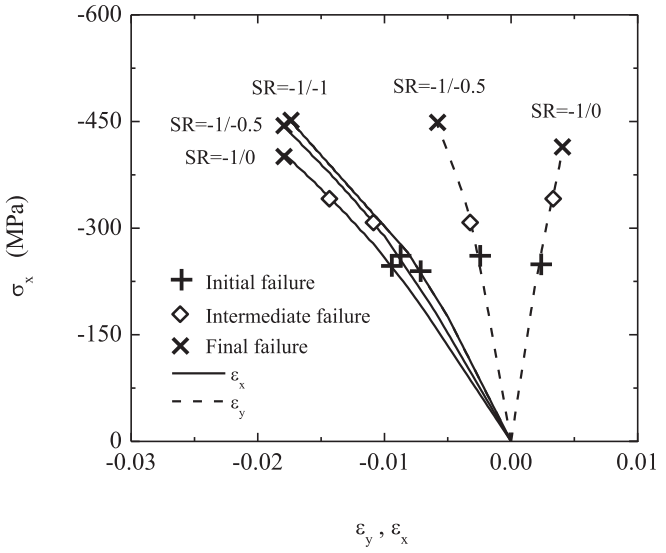

Fig. 19. Stress–strain curves of $[15/75]_s$ composite laminates subjected to biaxial compressions.

be seen that the area enclosed by each failure envelope is about the same. In addition, the longitudinal axial of the failure envelope rotates from 90° to 45° when the angle θ changes from 0° to 45°. Finally, these failure envelopes have a symmetric line of 45°. For example, the failure envelope of $[\pm35]_s$ composite laminate is symmetric to that of $[\pm55]_s$ composite laminate.

4.5. Composite laminates with symmetric cross-ply subjected to biaxial compressions

In this section, composite laminates with symmetric cross-ply $[\theta/(\theta-90)]_s$ subjected to biaxial compressions are investigated, where $\theta = 0°, 15°, 30°, 45°$. Typical loading paths of composite laminates for various SR ratios are shown in Fig. 6. Fig. 18 shows the stress and strain relations for $[0/90]_s$ composite laminates. When $SR = -1/0$ and $-1/-0.5$, the matrixes of the laminae with 90° fiber angle fail first due to the compression in the x direction, which is called the initial failure. When the loads are continuously increased, the matrixes of the laminae with 0° fiber angle also fail due to the compression in the y direction, which is called intermediate failure. Final failures of the laminates occur when the laminae with 0° fiber angle reach the ultimate compressive strength of the fiber. When $SR = -1/-1$, initial compressive failures take place at the matrixes of the laminae with 0° and 90° fiber angles simultaneously. Final failures of the laminate occur when the laminae with 0° and 90° fiber angles reach the ultimate compressive strength of the fiber simultaneously. It can be seen that the ultimate strengths of these laminates are independent of the SR ratio. The stress–strain curves of these laminates exhibit slightly nonlinear behavior after the intermediate failure occurs. This nonlinearity is due to the stress in the matrix being in the descending portion (Fig. 2d).

Fig. 19 shows the stress and strain relations for $[15/-75]_s$ composite laminates subjected to biaxial compressions. The stress–strain relations and failure patterns of $[15/-75]_s$ laminates are very

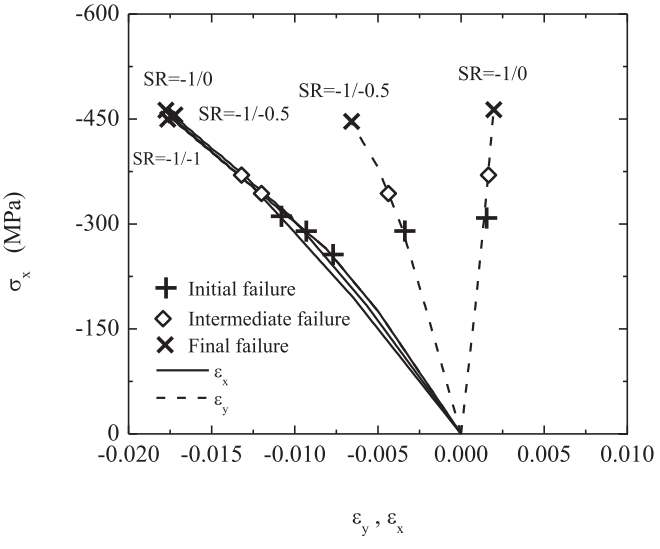

Fig. 18. Stress–strain curves of $[0/90]_s$ composite laminates subjected to biaxial compressions.

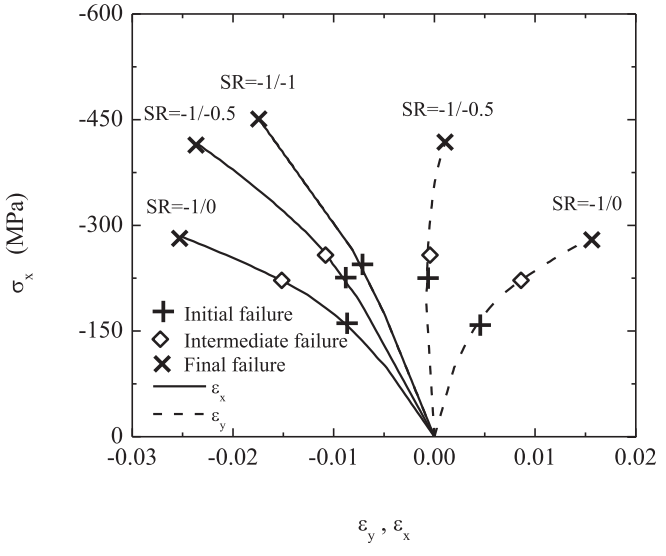

Fig. 20. Stress–strain curves of $[30/-60]_s$ composite laminates subjected to biaxial compressions.

similar to those of $[0/90]_s$ laminates. Fig. 20 shows the stress and strain relations for $[30/-60]_s$ composite laminates subjected to biaxial compressions. When SR = −1/0 and −1/−0.5, initial compressive failures occur at the matrixes of the laminae with a −60° fiber angle. Then intermediate compressive failures occur at the matrixes of the laminae with 30° fiber angle. The final failures occur when the in-plane shear stresses in the laminae with 30° and −60° fiber angles exceed the ultimate strength S (72 MPa) simultaneously. When SR = −1/−1, initial compressive failures occur at the matrixes of the laminae with 30° and −60° fiber angles simultaneously. Final failures of the laminate occur when the laminae with 30° and −60° fiber angles reach the ultimate in-plane shear strength simultaneously. It can be seen that the ultimate strengths of these laminates increase with the increase of the magnitude of compressive stress σ_y. The stress–strain curves of these laminates exhibit highly nonlinear behavior after the initial failure occurs. This nonlinearity is due to the nonlinear in-plane shear effect. The last composite laminate in analysis has the $[45/-45]_s$ layup. It is the same laminate as the $[\pm 45]_s$ composite laminate discussed in Section 4.2 and the stress–strain curves of the laminate with various SR ratios are already shown in Fig. 10.

Fig. 21 shows the failure stress σ_{xf} in the x direction versus the fiber angle θ for composite laminates with $[\theta/(\theta-90)]_s$ layup. It can be seen that all the curves are symmetric to a vertical line at θ = 45°. When $0° \le \theta \le 45°$, the failure stress usually decreases with the increase of the fiber angle θ. The exceptions are the curves with SR = −1/−1 and −1/−1.5. It should be noted that when SR = −1/−1, the stresses in the laminates are in a quasi-isotropic condition. Hence, it is not surprising to find that its failure stress is a constant for all angles θ. From this figure, we also observe that when SR changes from −1/0 to −1/−1, the failure stress increases with the increase of the magnitude of compressive stress σ_y. However, when SR changes from −1/−1 to −1/−10, the failure stress decreases with the increase of the magnitude of compressive stress σ_y.

4.6. Composite laminates with symmetric cross-ply subjected to biaxial tension and compression

In this section, composite laminates with symmetric cross-ply $[\theta/(\theta-90)]_s$ subjected to biaxial tension and compression are investigated. Typical loading paths of composite laminates for various SR ratios are shown in Fig. 6. Fig. 22 shows the stress and strain relations for $[0/90]_s$ composite laminates. It can be seen that all the stress–strain curves of the laminates with different SR ratios exhibit almost linear behavior both in the x and y directions. When SR = −1/0, initial compressive failure occurs at the matrix of the lamina with a 90° fiber angle. Then intermediate compressive failure takes place at the matrix of the lamina with a 0° fiber angle. Final failure of the laminate occurs when the lamina with a 0° fiber angle reach the ultimate compressive strength of the fiber. When SR = −1/0.5 and −1/1, the initial tensile failures occur at the matrixes of the laminae with a 0° fiber angle. Then intermediate compressive failures take place at the matrixes of the laminae with a 90° fiber angle. Final failures of the laminates occur when the laminae with a 0° fiber angle reach the ultimate compressive strength of the fiber. It can be seen that the ultimate strengths of these laminates are independent on the SR ratio.

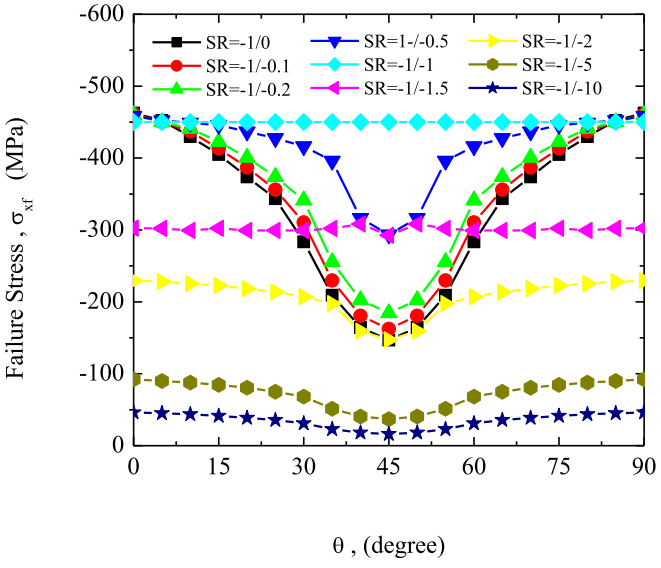

Fig. 21. Failure stress σ_{xf} versus angle θ for $[\theta/(\theta-90)]_s$ composite laminates subjected to biaxial compressions with various SR ratios.

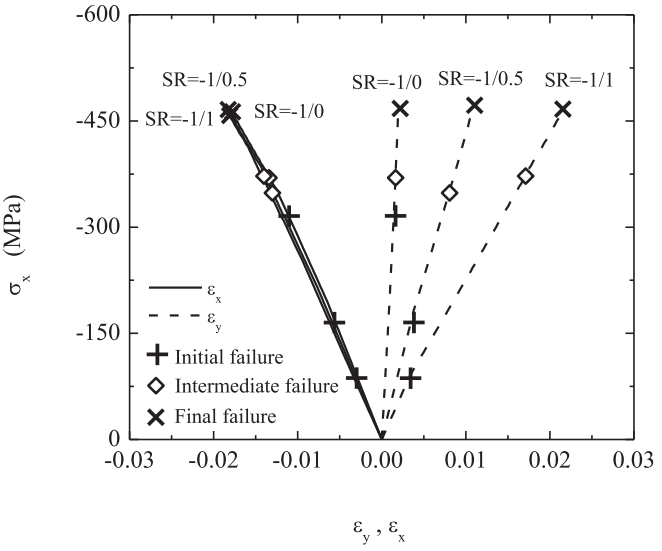

Fig. 22. Stress–strain curves of $[0/90]_s$ composite laminates subjected to biaxial tension and compression.

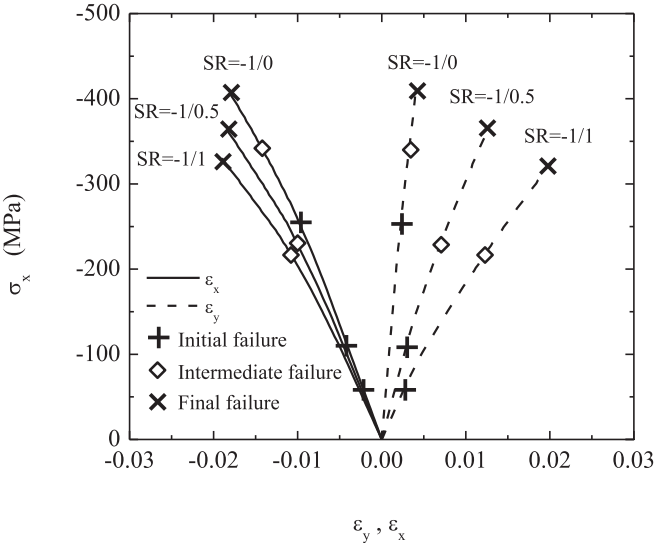

Fig. 23. Stress–strain curves of $[15/-75]_s$ composite laminates subjected to biaxial tension and compression.

Fig. 23 shows the stress and strain relations for $[15/-75]_s$ composite laminates subjected to biaxial tension and compression. It should be noted that all the failure modes of the $[15/-75]_s$ composite laminates are similar to those of the $[0/90]_s$ composite laminates for various SR ratios. We can see that Fig. 23 is similar to Fig. 22. All the stress–strain curves of the laminates with different SR ratios exhibit linear behavior both in the x and y directions before the initial failures occur. However, after the initial failures occur, these stress–strain curves exhibit slightly nonlinear behavior, which is due to the nonlinear shear effect. Again, the ultimate strengths of the laminates decrease with the increase of the magnitude of tensile stress σ_y.

Fig. 24 shows the stress and strain relations for $[30/-60]_s$ composite laminates subjected to biaxial tension and compression. Again, the ultimate strengths of the laminates decrease with the increase of the magnitude of tensile stress σ_y. When SR $= -1/0$, initial compressive failure occurs at the matrix of the lamina with a -60° fiber angle. Then intermediate compressive failure occurs at the matrix of the lamina with a 30° fiber angle. The final failures occur when the in-plane shear stresses in the laminae with 30° and -60° fiber angles exceed the ultimate strength S (72 MPa) simultaneously. When SR $= -1/0.5$ and $-1/1$, the initial compressive failures of the laminates occur at the matrixes of the laminae with a 30° fiber angle. Then intermediate compressive failures occur at the matrixes of the laminae with a -60° fiber angle. The final failures occur when the in-plane shear stresses in the laminae with 30° and -60° fiber angles exceed the ultimate strength S at the same time. Since the nonlinear in-plane shear effect is more significant, the stress–strain curves of these laminates exhibit more nonlinear behaviors than those of $[15/-75]_s$ laminates (Fig. 23). The last composite laminate in analysis has the $[45/-45]_s$ layup. It is the same laminate as the $[\pm 45]_s$ composite laminate discussed in Section 4.3 and the stress–strain curves of the laminate with various SR ratios are already shown in Fig. 15.

Fig. 25 shows the failure stress σ_{xf} in the x direction versus the fiber angle θ for composite laminates with $[\theta/(\theta-90)]_s$ layup. It can be seen that all the curves are symmetric to a vertical line at $\theta = 45^\circ$. When $0^\circ \le \theta \le 45^\circ$, the failure stress decrease with the increase of the fiber angle θ. From this figure, we also observe that the failure stress decrease with the increase of the magnitude of tensile stress σ_y.

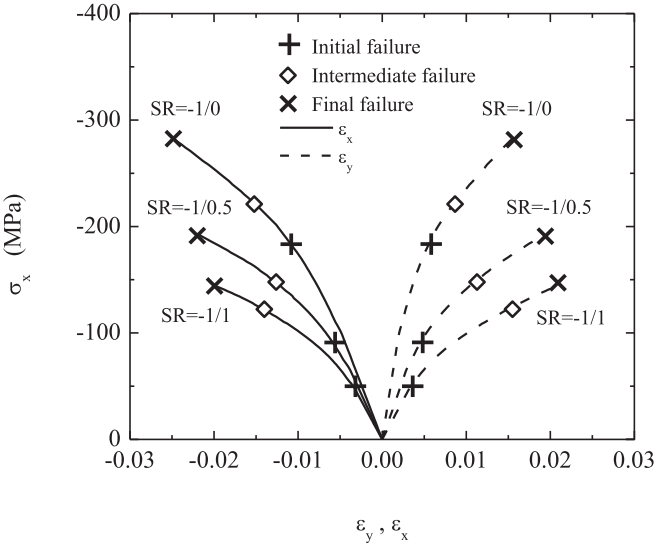

Fig. 24. Stress–strain curves of $[30/-60]_s$ composite laminates subjected to biaxial tension and compression.

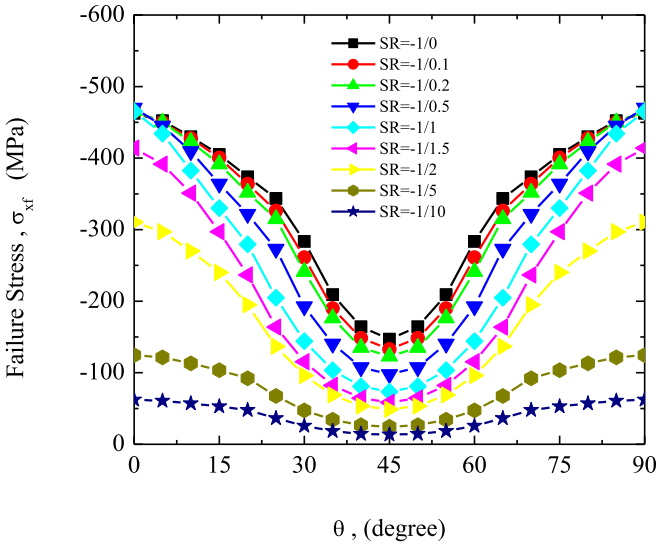

Fig. 25. Failure stress σ_{xf} versus angle θ for $[\theta/(\theta-90)]_s$ composite laminates subjected to biaxial tension and compression with various SR ratios.

4.7. Failure envelopes of biaxial stresses for composite laminates with symmetric cross-ply

The stress–strain curves and failure patterns of the composite laminates with symmetric cross-ply $[\theta/(\theta-90)]_s$ subjected to biaxial tensions are similar to those of the laminates subjected to biaxial compressions as discussed in Section 4.5. Hence, they are not duplicated here. Again it should be noted that the ultimate strengths of the laminates subjected to biaxial tensions are large than those of the same laminates subjected to biaxial compressions.

Finally, the failure envelopes of biaxial stresses for composite laminates with symmetric cross-ply $[\theta/(\theta-90)]_s$ are given in Fig. 26. It can be seen that all the failure envelopes pass through the same two points, in which SR $= 1/1$ and $-1/-1$. In addition, each failure envelope is symmetric to the line of 45° by itself. Finally, the area enclosed by the failure envelope decreases as the angle θ increases. This means that the $[0/90]_s$ laminate can resist more wide combinations of σ_x and σ_y without failure than the $[15/-75]_s$, $[30/-60]_s$ and $[45/-45]_s$ laminates.

5. Conclusions

This paper presents a material constitutive model suitable for the failure analysis of composite laminates under biaxial loads. The validity of the constitutive model has been verified against the experimental data [56] and reasonable accuracy has been achieved. Based on the numerical analyses of symmetric angle-ply composite laminates and symmetric cross-ply composite laminates subjected to biaxial loads, the following conclusions could be made:

1. For composite laminates with symmetric angle-ply $[\pm\theta]_s$ subjected to biaxial compressions, the optimal fiber angle of the laminate change from 0° to 90°, as the SR ratio changes from $-1/0$ to $-1/-25$. When $\theta = 0^\circ$ or $75^\circ \le \theta \le 90^\circ$, the failure stress decreases with the increase of the magnitude of the compressive stress σ_y. When $5^\circ \le \theta \le 70^\circ$, the failure stress depends on the SR ratio significantly.
2. For composite laminates with symmetric angle-ply $[\pm\theta]_s$ subjected to biaxial tension and compression, the optimal fiber angle changes from 0° to 90°, as the SR ratio changes from $-1/$

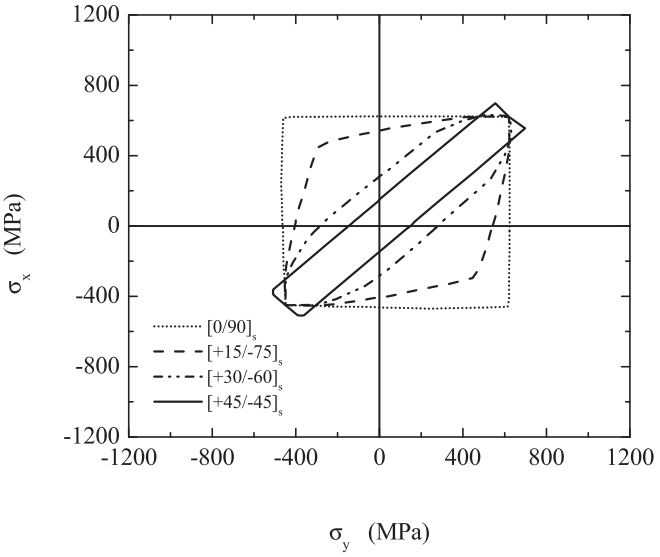

Fig. 26. Failure envelopes of biaxial stresses for $[\theta/(\theta-90)]_s$ composite laminates.

0 to −1/20. The failure stress decreases with the increase of the magnitude of the tensile stress σ_y. This decrease of the failure stress in magnitude is more significant for small angles (say $0^\circ \le \theta \le 15^\circ$) than that for large angles (say $75^\circ \le \theta \le 90^\circ$)

3. For composite laminates with symmetric angle-ply $[\pm\theta]_s$ subjected to biaxial stresses, the area enclosed by each failure envelope is about the same. The longitudinal axial of the failure envelope rotates from 90° to 45° when the fiber angle θ changes from 0° to 45°. In addition, these failure envelopes have a symmetric line of 45°. For example, the failure envelope of $[\pm35]_s$ composite laminate is symmetric to that of $[\pm55]_s$ composite laminate.
4. For composite laminates with symmetric cross-ply $[\theta/(\theta-90)]_s$ subjected to biaxial compressions, all the curves of failure stress versus fiber angle θ are symmetric to a vertical line at $\theta = 45^\circ$. When $0^\circ \le \theta \le 45^\circ$, the failure stress usually decreases with the increase of the fiber angle θ. The exceptions are the curves with SR = −1/−1 and −1/−1.5. When the SR ratio changes from −1/0 to −1/−1, the failure stress increases with the increase of the magnitude of compressive stress σ_y. However, when SR changes from −1/−1 to −1/−10, the failure stress decreases with the increase of the magnitude of compressive stress σ_y.
5. For composite laminates with symmetric cross-ply $[\theta/(\theta-90)]_s$ subjected to biaxial tension and compression, all the curves of failure stress versus fiber angle θ are symmetric to a vertical line at $\theta = 45^\circ$. When $0^\circ \le \theta \le 45^\circ$, the failure stress decrease with the increase of the fiber angle θ. In addition, the failure stress decrease with the increase of the magnitude of tensile stress σ_y.
6. For composite laminates with symmetric cross-ply $[\theta/(\theta-90)]_s$ subjected to biaxial stresses, each failure envelope is symmetric to the line of 45° by itself. In addition, the area enclosed by the failure envelope decreases as the fiber angle θ increases.

References

[1] Chang FK, Chang KY. A progressive damage model for laminated composites containing stress concentrations. J Compos Mater 1987;21(9):834–55.
[2] Hu H-T. Influence of in-plane shear nonlinearity on buckling and postbuckling responses of composite laminate plates and shells. J Compos Mater 1993;27(2):138–51.
[3] Edge EC. Stress based Grant-Sanders method for predicting failure of composite laminates. Compos Sci Technol 1998;58(7):1033–41.
[4] Hinton MJ, Soden PD. Predicting failure in composite laminates: background to the exercise. Compos Sci Technol 1998;58(7):1001–10.
[5] Liu KS, Tsai SW. A progressive quadratic failure criterion for a laminate. Compos Sci Technol 1998;58(7):1023–32.
[6] Sun CT, Tao JX. Prediction of failure envelopes and stress/strain behaviour of composites laminates. Compos Sci Technol 1998;58(7):1125–36.
[7] Ferry L, Perreux D, Rousseau J, Richard F. Interaction between plasticity and damage in the behaviour of $[+\phi,-\phi]_n$ fibre reinforced composite pipes in biaxial loading (internal pressure and tension). Compos Part B Eng 1998;29(6):715–23.
[8] Gummadi LNB, Palazotto AN. Progressive failure analysis of composite cylindrical shells considering large rotations. Compos Part B Eng 1998;29(5):547–63.
[9] Spootswood MS, Palazotto AN. Progressive failure analysis of a composite shell. Compos Struct 2001;53(1):117–31.
[10] Maa RH, Cheng JH. A CDM-based failure model for predicting strength of notched composite laminates. Compos Part B Eng 2002;33(6):479–89.
[11] Lin W-P, Hu H-T. Nonlinear analysis of fiber-reinforced composite laminates subjected to uniaxial tensile load. J Compos Mater 2002;36(12):1429–50.
[12] Lin W-P, Hu H-T. Parametric study on the failure of fiber-reinforced composite laminates under biaxial tensile load. J Compos Mater 2002;36(12):1481–504.
[13] Hu H-T, Yang C-H, Lin F-M. Buckling analyses of composite laminate skew plates with material nonlinearity. Compos Part B Eng 2006;37(1):26–36.
[14] Liu PF, Zheng JY. Progressive failure analysis of carbon fiber/epoxy composite laminates using continuum damage mechanics. Mater Sci Eng A 2008;485(1–2):711–7.
[15] Labeas G, Belesis S, Stamatelos D. Interaction of damage failure and post-buckling behaviour of composite plates with cut-outs by progressive damage modelling. Compos Part B Eng 2008;39(2):304–15.
[16] Tay TE, Liu G, Tan VBC, Sun XS, Pham DC. Progressive failure analysis of composites. J Compos Mater 2008;42(18):1921–66.
[17] Liu PF, Zheng JY. Recent developments on damage modeling and finite element analysis for composite laminates: a review. Mater Des 2010;31(8):3825–34.
[18] Lim W-K, Jeong W-K, Tschegg EK. Failure of fibrous anisotropic materials under combined loading. Compos Part B Eng 2010;41(1):94–7.
[19] Maimi P, Camanho PP, Mayugo JA, Turon A. Matrix cracking and delamination in laminated composites. Part I: ply constitutive law, first ply failure and onset of delamination. Mech Mater 2011;43(4):169–85.
[20] Kumar D, Singh SB. Stability and failure of composite laminates with various shaped cutouts under combined in-plane loads. Compos Part B Eng 2012;43(2):142–9.
[21] Zhang BM, Zhao L. Progressive damage and failure modeling in fiber-reinforced laminated composites containing a hole. Int J Damage Mech 2012;21:893–911.
[22] Pham DC, Sun XS, Tan VBC, Chen B, Tay TE. Progressive failure analysis of scaled double-notched carbon/epoxy composite laminates. Int J Damage Mech 2012;21(8):1154–85.
[23] Anyfantis KN, Tsouvalis NG. Post buckling progressive failure analysis of composite laminated stiffened panels. Appl Compos Mater 2012;19(3–4):219–36.
[24] Cárdenasa D, Elizaldeb H, Marzoccac P, Abdid F, Minnetyane L, Probst O. Progressive failure analysis of thin-walled composite structures. Compos Struct 2013;95:53–62.
[25] Yang QJ, Hayman B, Osnes H. Simplified buckling and ultimate strength analysis of composite plates in compression. Compos Part B Eng 2013;54:343–52.
[26] Wang F, Ding J, Chen Z. Statistical analysis of the progressive failure behavior for fiber-reinforced polymer composites under tensile loading. Polymers 2014;6(1):145–59.
[27] Chróścielewski J, Kreja I, Sabik I, Sobczyk B, Witkowski W. Failure analysis of footbridge made of composite materials. In: Pietraszkiewicz W, Gorski J, editors. Shell structures: theory and application, vol. 3; 2014. p. 389–96.
[28] Liu PF, Xing LJ, Zheng JY. Failure analysis of carbon fiber/epoxy composite cylindrical laminates using explicit finite element method. Compos Part B Eng 2014;56:54–61.
[29] Chen X, Li Z, Wang H. Progressive failure analysis of an open-hole composite laminate by using the S-version finite-element method. Mech Compos Mater 2014;50(3):279–94.
[30] Turan K, Gur M, Kaman MO. Progressive failure analysis of pin-loaded unidirectional carbon-epoxy laminated composites. Mech Adv Mater Struct 2014;21(2):98–106.
[31] Lee C-S, Kim J-H, Kim S-K, Ryu D-M, Lee J-M. Initial and progressive failure analyses for composite laminates using puck failure criterion and damage-coupled finite element method. Compos Struct 2015;121:406–19.
[32] Lee S-Y, Roh J-H. Two-dimensional strain-based interactive failure theory for multidirectional composite laminates. Compos Part B Eng 2015;69:69–75.
[33] Hahn HT, Tsai SW. Nonlinear elastic behavior of unidirectional composite laminae. J Compos Mater 1973;7(1):102–18.
[34] Paepegem WV, Baere ID, Degrieck J. Modelling the nonlinear shear stress-strain response of glass fibre-reinforced composites. Part I: experimental results. Compos Sci Technol 2006;66(10):1455–64.
[35] Petit PH, Waddoups ME. A method of predicting the nonlinear behavior of laminated composites. J Compos Mater 1969;3(1):2–19.

[36] Jones RM, Morgan HS. Analysis of nonlinear stress-strain behavior of fiber-reinforced composite materials. AIAA J 1977;15(12):1669–76.
[37] Bogetti TA, Hoppel CPR, Harik VM, Newill JF, Burns BP. Predicting the nonlinear response and progressive failure of composite laminates. Compos Sci Technol 2014;64(3–4):329–42.
[38] Griffin OH, Kamat MP, Herakovich CT. Three-dimensional inelastic finite element analysis of laminated composites. J Compos Mater 1981;15(6):543–60.
[39] Kenaga D, Doyle JF, Sun CT. The characterization of boron/aluminum composite in the nonlinear range as an orthotropic elastic-plastic material. J Compos Mater 1987;21(6):516–31.
[40] Sun CT, Chen JL. A simple flow rule for characterizing nonlinear behavior of fiber composite. J Compos Mater 1989;23(10):1009–20.
[41] Vaziri R, Olson MD, Anderson DL. A plasticity-based constitutive model for fibre-reinforced composite laminates. J Compos Mater 1991;25(5):512–35.
[42] Nanda A, Kuppusamy T. Three-dimensional elastic-plastic analysis of laminated composite plates. Compos Struct 1991;17(3):213–25.
[43] Allen H, Harris CE, Groves SE. A thermomechanical constitutive theory for elastic composites with distributed damage-I, theoretical development. Int J Solids Struct 1987;23(9):1301–18.
[44] Rowlands RE. Strength (failure) theories and their experimental correlation. In: Sih GC, Skudra AM, editors. Failure mechanics of composites. Elsevier; 1985. pp.71–125.
[45] Hoffman O. The brittle strength of orthotropic materials. J Compos Mater 1967;1(2):200–6.
[46] Tsai SW, Wu EM. A general theory of strength for anisotropic materials. J Compos Mater 1971;5(1):58–80.
[47] Lee JD. Three dimensional finite element analysis of damage accumulation in composite laminate. Comput Struct 1982;15(3):335–50.
[48] Chang FK, Lessard LB. Damage tolerance of laminated composite containing an open hole and subjected to compressive loadings: part I-analysis. J Compos Mater 1991;25(1):2–43.
[49] Rotem A. Prediction of laminate failure with the rotem failure criterion. Compos Sci Technol 1998;58(7):1083–94.
[50] Groenwold AA, Haftka RT. Optimization with non-homogeneous failure criteria like Tsai-Wu for composite laminates. Struct Multidiscip Optim 2006;32(3):183–90.
[51] Zhu H, Sankar BV. Evaluation of failure criteria for fiber composites using finite element micromechanics. J Compos Mater 1998;32(8):766–82.
[52] Dassault Systèmes Corporation. SIMULIA abaqus analysis user's manuals, theory manuals and example problems manuals, version 6.14. 2014. France.
[53] Mindlin RD. Influence of rotatory inertia and shear on flexural motions of isotropic elastic plate. J Appl Mech 1951;18:31–8.
[54] Narayanaswami R, Adelman HM. Evaluation of the tensor polynomial and Hoffman strength theories for composite materials. J Compos Mater 1977;11(4):366–77.
[55] Ke L-S. Constitutive modelling of fiber-reinforced composite laminates subjected to uniaxial compressive loads [M.S. thesis]. Tainan, Taiwan, R.O.C: Department of Civil Engineering, National Cheng Kung University; 2002.
[56] Soden PD, Kitching R, Tse PC. Experimental failure stresses for ±55° filament wound glass fiber reinforced plastic tubes under biaxial loading. Composites 1989;20(2):125–35.
[57] Soden PD, Hinton MJ, Kaddour AS. Lamina properties, lay-up configurations and loading conditions for a range of fibre reinforced composite laminates. Compos Sci Technol 1998;58(7):1011–22.